Behavior of Giant Vesicles with Anchored DNA Molecules

Vesselin Nikolov, Reinhard Lipowsky, and Rumiana Dimova
Max Planck Institute of Colloids and Interfaces, 14424 Potsdam, Germany

ABSTRACT We study changes in curvature and elastic properties of lipid membranes induced by anchoring of long hydrophilic polymers at low polymer surface concentrations (corresponding to the mushroom regime). The effect of anchored polymers on the membrane spontaneous curvature is characterized by monitoring the changes in the fluctuation spectra and the morphology of giant unilamellar vesicles. The polymers used in our study are fluorescently labeled and biotinylated λ-phage DNA molecules which bind to biotinylated giant unilamellar vesicles via a biotin-avidin-biotin linkage. By varying the amount of biotinylated lipid in the membrane, we control the surface concentration of anchors. At low anchor concentrations, the spontaneous curvature of the membrane increases linearly with the DNA concentration. The linear increase is consistent with theoretical predictions for polymer surface concentrations in the mushroom regime. At higher anchor concentrations, which should still belong to the mushroom regime, the vesicles undergo budding transitions. In this latter regime, the bud size is used to estimate the polymer-induced membrane curvature.

INTRODUCTION

Every membrane can be characterized by an inherent spontaneous curvature, which determines the preferred direction of bending. The concept of spontaneous curvature was first introduced for monolayers by Bancroft and Tucher (1) and later elaborated for bilayers by Helfrich (2). Numerous studies have shown that the membrane spontaneous curvature is an important parameter, which determines the morphology of lipid vesicles (3,4) and polymerosomes (5,6), influences the functioning of some transmembrane proteins (7), and plays a role in biological processes, such as membrane fusion (8). Giant unilamellar vesicles (GUVs) are closed membrane sacks, encompassing fluid media with a linear size in the range of 5–100 μm. In general, their spontaneous curvature is close to zero, because the membrane is locally flat. A nonzero spontaneous curvature can be induced by a variety of mechanisms (9) such as an unequal number or mismatch in the headgroup area of the molecules composing each of the two leaflets of the bilayer (10), asymmetry in the particle type or solution composition on both sides of the membrane (11–13), flip-flop, pH or charge asymmetry (14–16), etc.

The spontaneous curvature induced by asymmetric grafting of polymers on the membrane is a property of special interest, because the plasma membrane of living cells is associated with a large number of asymmetrically distributed or anchored polymers. The intracellular leaflet of the membrane is connected to the polymer network of the cytoskeleton, which determines the membrane shape. The extracellular side is covered with anchored receptors and polysaccharides, which form the so-called glycocalix. In addition to their various biological functions, all anchored polymers tend to curve the membrane and, thus, to induce a spontaneous membrane curvature.

In this article, we are concerned with the presumably simplest polymer/membrane architecture: we study flexible polymers for which one end provides the membrane anchor whereas all other polymer segments experience effectively repulsive interactions with the membrane. The anchored polymers then form mushrooms at low surface concentrations and brush states at high surface concentrations (17,18). In this article, we will be only concerned with the mushroom regime.

A single mushroom anchored to the membrane exerts an entropic pressure onto the adjacent membrane segment that bends it away from the polymer (17–22). As a result, the membrane segment assumes a conical shape close to the anchor point, which relaxes into a catenoidlike shape further away from this point. In addition, the polymer mushrooms also increase the bending rigidity of the membranes (18,22). The latter effect has been confirmed experimentally in microemulsions (23).

The spontaneous curvature induced by single mushrooms grows linearly with the surface concentration of the polymers (18,19). As the surface concentration of the anchored polymers is increased, the lateral diffusion of these polymers leads to more frequent collisions between them. These polymer/polymer collisions give rise to another contribution to the spontaneous curvature of the membrane that is quadratic in the surface concentration of the polymers (19,24).

Membrane curvature induced by anchored polymers has also been studied experimentally by several groups (10,25–29).

In an attempt to develop a suitable platform for drug delivery, Blume and Cevc (25) studied the circulation in the blood stream of lipid vesicles sterically stabilized with hydrophilic polymers. Membranes shielded by grafted polyethylene glycol covalently attached to lipid molecules are long known as stealth liposomes used in drug delivery (30). Model lipid

Submitted October 30, 2006, and accepted for publication February 13, 2007.

Address reprint requests to R. Dimova, Tel.: 49-331-567-9615; E-mail: dimova@mpikg.mpg.de.

0006-3495/07/06/4356/13 $2.00

doi: 10.1529/biophysj.106.100032

membranes lack the stabilizing polymer network of the cytoskeleton in cell membranes. To simulate biological membranes and to improve the mechanical stability of model membranes, Ringsdorf et al. (26) (see also (31)) mimicked the cytoskeleton with thermoactive polymers anchored to lipid membranes. The elastic stretch and bending rigidity of membranes decorated with water-soluble polymers was characterized using the micropipette aspiration technique (32). The physicochemical properties of lipid membranes with grafted polymers were generalized in a recent review (33).

Of particular interest among reports on polymer-grafted membranes are the studies performed on giant unilamellar vesicles (GUVs) because these reflect the membrane behavior on the size scale of the cell. In addition, their shape and fluctuations encode information about the bilayer spontaneous curvature (16,34,35). Polymer anchoring was observed to induce dramatic changes in the vesicle shape (10,27) and pearling instability (28,29). Despite the obvious relevance of the polymer-induced spontaneous curvature, the latter has not yet been systematically studied and quantified experimentally.

Finding an appropriate model system for measuring the polymer-induced spontaneous curvature of the lipid membrane is a nontrivial task. In particular, the choice for the polymers is not straightforward since their properties should meet certain requirements that are difficult to fulfill. First, the macromolecules should be well characterized in terms of their functional groups (charge and/or hydrophilicity), total chain length, flexibility, i.e., persistence length, etc. Second, it would be advantageous if the polymer backbone allows for fluorescent labeling and is sufficiently long to be directly observed with optical microscopy. The fluorescence from such long polymers anchored to the membrane should be detectable for characterizing the polymer surface concentration. However, two of these requirements, fixed total chain length and long backbone, are difficult to meet for synthetic macromolecules, which exhibit a certain polydispersity in molecular weight and polymer length. Another requirement is that the polymer needs to have an anchor segment by which it can be attached to the membrane (see, e.g., Fig. 1 *A*). This necessitates certain chemical modifications of the polymer usually associated with covalent binding of a hydrophobic segment that would insert in the membrane. The concentration of anchored polymers at the membrane surface is determined by the partitioning of the polymer between the bulk solution and the lipid membrane (36), i.e., by the polymer bulk concentration and the equilibrium constant of the adsorption/anchoring process (see Fig. 1 *A*). In addition, insertion of such a polymer into the membrane induces a change in the area of the external leaflet thus altering the spontaneous curvature of the bilayer and making it difficult to decouple this effect from the anchored polymer entropic contribution to the curvature change. A possible solution is to use anchoring sites in the membrane to which the polymers would bind (see Fig. 1 *B*).

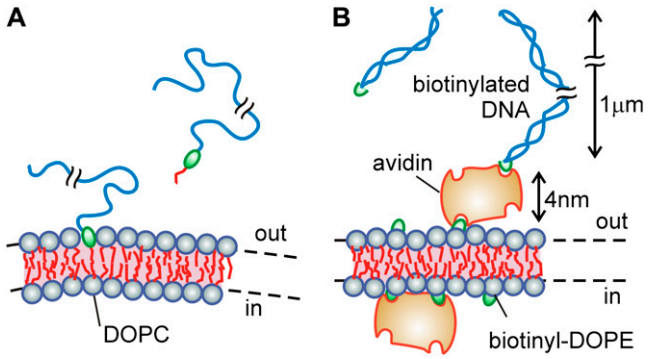

FIGURE 1 (*A*) Insertion of a polymer with an anchor segment to the external leaflet of a lipid membrane. (*B*) Anchoring of a polymer (biotinylated DNA) to a membrane already containing the anchoring sites such as avidin attached to a biotinylated membrane.

In an attempt to meet all of the above requirements, we have chosen λ-phage DNA as a long and well-defined polymer. The advantages are as follows:

1. DNA can be reproducibly purified and is always monodisperse. Thus, all polymers are identical and have the same fixed length. The relatively large contour length of the DNA, which is ~14 μm in the stretched state, makes the molecule an attractive model polymer suitable for single molecule experiments (see, e.g., (37,38)).
2. DNA can be fluorescently labeled. Useful fluorescent dyes that easily intercalate into the DNA backbone are the dimeric cyanine dyes TOTO-1 and YOYO-1 (39). This usually leads to an increase in the polymer length by up to ~30% but without a noticeable change in the persistence length of the polymer (40). Due to the large size, single-labeled λ-phage DNA molecules can then be visualized and manipulated (see, e.g., (41,42)).
3. λ-phage DNA can be chemically modified to create an anchoring segment at one end. This DNA molecule has two single-stranded overhangs of 12 nucleotides on each 5′-end, called ''sticky'' ends. Using an appropriate set of enzymes, one can ligate an oligo-nucleotide, which is complementary to one of the ends and is already modified to contain the anchoring segment.
4. Finally, by using electrolyte solutions of various concentrations, the interaction between the negatively charged phosphate groups along the DNA backbone can be modulated or completely screened.

Using DNA as a model polymer, we characterize the effect on the membrane spontaneous curvature, which arises from grafting of polymers on one side of the membrane of a giant vesicle. In our systems, each polymer is firmly attached to the membrane by a lipidlike anchor, which is covalently bound to one end of the polymer. We gradually increase the surface concentration of the anchored polymers, keeping precise control on the number of anchors on the membrane surface.

The polymer-induced spontaneous curvature is measured using polymer-free membranes as a reference system. The article is organized as follows. In the next section, we introduce the experimental approach and describe the procedures and data analysis. Afterwards we briefly discuss the theoretical bases of accessing the membrane spontaneous curvature from the experimental data. Then the results are presented, followed by some concluding remarks.

MATERIALS, METHODS, AND EXPERIMENTAL PROCEDURE

The attachment of DNA to the GUV membrane was achieved in the following way. One end of the DNA was biotinylated (described in the section DNA Biotinylation and Fluorescent Labeling). The vesicles contained biotinylated lipids. Avidin, being able to bind up to four biotin groups, was used as a linker between the biotinylated membrane and the DNA. The concentration of biotinylated lipids, which played the role of anchoring sites in the membrane, determined the surface concentration of anchored DNA.

The biotinylated vesicles were grown in avidin solution using the procedure described in the following section. The binding of avidin to the biotinylated membrane is characterized by a specific equilibrium constant, determined in an independent study using isothermal titration calorimetry (43) (the data will be published elsewhere). The equilibrium constant is relatively high, indicating that when vesicles are grown in the presence of a large excess of avidin (relative to the biotin concentration), all biotin sites on the membrane surface are bound by avidin. The vesicles, with a fixed amount of avidin on the surface, were then transferred to the observation chamber, where the biotinylated DNA was consequently introduced. The fluctuation spectrum of a selected vesicle was detected and analyzed before and after introducing the DNA solution.

Vesicle preparation

1,2-dioleoyl-*sn*-glycero-3-phosphocholine (DOPC) and 1,2-dioleoyl-*sn*-glycero-3-phosphoethanolamine-*n*-cap biotinyl (Biotinyl-Cap-PE) were purchased from Avanti Polar Lipids (Alabaster, AL) and used without further purification. Giant unilamellar vesicles were prepared by spontaneous swelling as described previously (13,44). Briefly, chloroform solutions of the two lipids at ratios of DOPC/biotinyl-Cap-PE ranging from 10^6:1 to 10^7:1 were prepared. Several droplets (30 μl) of the solution were deposited on a roughened Teflon plate and spread with the tip of a Hamilton syringe. The solvent was evaporated under vacuum overnight and the plate was hydrated for 8–10 h in water vapor atmosphere at 37°C. Sucrose solution of avidin in buffer (10 mM HEPES, 5 mM ascorbic acid, pH 7) with overall osmolarity between 150 and 200 mOsm/kg was added to the vessel with the Teflon plate. The bulk avidin concentration was in excess (100 times larger) relative to the concentration of biotinyl-Cap-PE. A characteristic cloud of concentrated vesicle suspension in the vessel was observed within 24–30 h. The vesicles were then carefully taken out and diluted in glucose buffer (used as a solvent for the DNA solutions, see below) of the same osmolarity as the vesicle sucrose solution. Because the avidin-biotin bond is very strong ($\sim$35 k_BT, where k_BT is the thermal energy), no dissociation of the formed avidin-vesicle complex is expected to occur as the solution is diluted. Due to the refractive index difference between the internal vesicle sucrose solution and the external media glucose solution, the GUVs could easily be observed with an optical microscope in phase contrast mode. In addition, the density difference of these solutions caused the vesicles to settle at the bottom of the experimental chamber, thus further facilitating the observation. On the average, the GUVs were polydisperse with a typical size between 5 and 20 μm.

DNA biotinylation and fluorescent labeling

Double-stranded λ-phage DNA was purchased from Fermentas (St. Leon-Rot, Germany). The molecule represents the whole genome of the bacteriophage Lambda (45). Each DNA molecule has single-stranded overhangs of 12 nucleotides on each 5′-end. One of these overhangs was ligated with a biotinylated complementary nucleotide with sequence 5′-GGG-CGG-CGA-CCT-biotin-3′ (MWG-Biotech, Ebersberg, Germany). The ligation protocol was similar to the protocol developed in the literature (46,47). Before ligation, the DNA molecules (0.42 nM) were dephosphorylated with alkaline phosphatase (New England Biolabs, Frankfurt, Germany), which afterwards was inactivated according to the procedure prescribed by the manufacturer. The dephosphorylated molecules were incubated together with the oligonucleotides in T4 ligase buffer (New England Biolabs) for 3 h at 21°C. The biotinylated DNA molecules were then fluorescently labeled with TOTO-1 (513/531) (Molecular Probes, Eugene, OR) at ratio 1:5 TOTO-1:bp. The dye is essentially not fluorescent except when bound to DNA. The TOTO-1 molecule has very high affinity for nucleic acids (48) and thus dissociation of the dye-DNA complex is unlikely to occur in the dilute solutions needed to resolve single molecules.

Setup and experimental steps

The experiments were performed in a homemade flow chamber (see Fig. 2) constructed in the following way. A Teflon frame with in/out channels was fixed on one side to the glass window of a hollow metal holder, and on the other side it was sealed with a microscope cover glass. The metal holder, with water running through it, connected to a thermostat, allowed for maintaining the temperature inside the flow chamber at 25°C $\pm$ 0.1°C. Temperature stability was important because observation times were long ($\geq$5 h) and fluctuation spectra can be influenced by small temperature drifts. The enclosed volume of the Teflon frame chamber ($\sim$500 μl) was connected with a pipe to an external vessel containing the studied solution. Another pipe connected the chamber outlet to a computer-controlled micropump (Lee Hydrau lische Miniatur Komponeten GmbH, Frankfurt, Germany), which allowed for smooth exchange of the solution in the chamber by applying a small suction pressure. During this exchange, the microscope stage was repositioned correspondingly to follow a vesicle of interest and to keep it in the field of view.

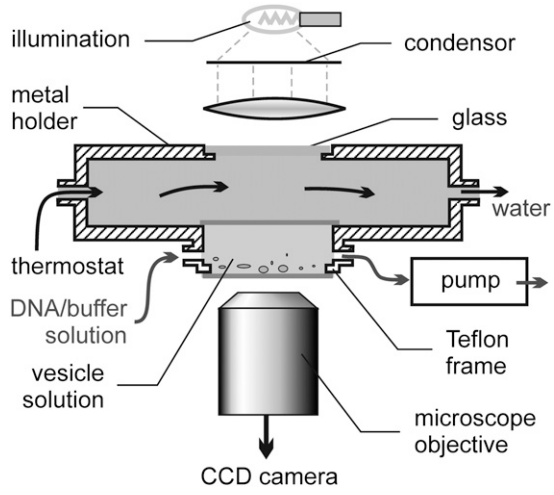

FIGURE 2 Schematic sketch of the experimental setup with a cross section of the homemade flow chamber. The latter is connected to a pump, which allows for exchange of the solutions inside the chamber. The vesicles are initially introduced in the chamber. After equilibration, the external media is gradually exchanged with buffer or DNA solution. A water jacket assures constant temperature in the chamber. The length of the chamber is $\sim$1.5 cm. The dimensions are not in scale.

To prevent the vesicles from adhesion to the glass walls we coated the chamber interior in the following way (the vesicles did adhere to nonpretreated glass). The flow chamber was filled with 1 mg/ml albumin solution (Sigma-Aldrich, St. Louis, MO). The protein was allowed to adsorb for 15 min. The excess albumin was rinsed out by flushing 4 ml buffer solution. Afterwards, the vesicle solution was introduced in the flow chamber. To avoid temperature-induced effects, the whole experimental setup was equilibrated for 1 h before the experiment was started. During this time, due to the inside/outside density difference of the vesicle solutions (1.0235 g/cm^3 for sucrose inside and 1.0115 g/cm^3 for glucose solutions outside of 200 mM concentration), the vesicles sunk to the bottom of the flow chamber. As mentioned before, due to the refractive index difference of sucrose and glucose (1.3424 and 1.3380, respectively, for 200 mM solutions), the contrast of the obtained images was enhanced. The vesicles appear as dark objects with bright halo on a light-shaded background.

The microchamber was scanned for a fluctuating prolate unilamellar and defect-free vesicle. To assess the curvature effect induced by the polymer only, we had to compare it to the inherent membrane curvature in the absence of polymer. To achieve this, we used the following three-step procedure. First, we examined the stability of the fluctuation spectra of a certain vesicle membrane over a time period of ~30–60 min. If the fluctuation spectra were not stable, the vesicle was discarded, another one was selected, and the procedure was repeated. This ensures that the selected vesicle was thermodynamically equilibrated within the timescale of the experiments. Second, we flushed in buffer (200 μl/min) to test the vesicle response toward shear stress. This was a necessary step to distinguish the shear effect of flushing DNA solution from the effect of anchoring the molecules onto the vesicle membrane. The shear test was also helpful to detect whether the vesicle was in some way attached or partially adhered to the glass surface of the chamber. When the vesicle did not drift in the direction of the flow of injected buffer, or showed dramatic change in the fluctuation spectra, it was assumed to be attached to the glass and was discarded. The fraction of vesicles in the chamber, which did not exhibit any of those deficiencies, was far below 1%. Finally, when the fluctuation spectrum remained unaffected by the shear stress, the DNA solution ($\sim 10^{-13}$ M) was flushed through the chamber (200 μl/min or slower). The vesicle fluctuations were analyzed and the effect induced by the DNA was extracted from the changes in the fluctuations spectrum.

Fluctuation spectroscopy of prolate vesicles: spontaneous curvature

At room temperature, all nonspherical vesicles undergo detectable thermal fluctuations. The area available for fluctuations or shape changes depends on the dimensionless volume/area ratio,

$$v \equiv (3V/4\pi)(A/4\pi)^{-3/2}, \tag{1}$$

where V and A are the vesicle volume and area, respectively (a spherical vesicle is characterized by reduced volume $v = 1$). The fluctuation spectrum depends on the bending stiffness κ and the spontaneous curvature of the membrane, M_{sp}. The complete procedure of detection and analysis of the fluctuations of elongated prolate vesicles is described in detail elsewhere (34,35). Briefly, a selected vesicle is observed with a CCD camera (model No. C5985-10, Hamamatsu, Hamamatsu City, Japan) and video-recorded. The images are simultaneously digitized and processed by an SGI Indy workstation (Silicon Graphics, Sunnyvale, CA). A closed contour around a vesicle is detected from the analysis of the shaded values of the image (the algorithm needs between 0.4 and 0.6 s to trace a contour, depending on the vesicle image size). The contour, in polar coordinates (R, φ), is then expanded in Fourier series around the equivalent sphere radius, R_0, of the vesicle:

$$R(\varphi) = R_0\left[1 + \sum_n a_n \cos(n\varphi) + \sum_n b_n \sin(n\varphi)\right]. \tag{2}$$

The amplitudes $\{a_n, b_n\}$ are numerically calculated (see (35)). Their mean values describe the geometry of the vesicle, e.g., for a prolate vesicle $\langle a_2\rangle$ reflects the elongation or ellipticity of the vesicle, and $\langle a_3\rangle$ describes the asymmetry across the plane of up/down symmetry of the prolate. A quantity characterizing the thermal fluctuations is the mean-square average value of the amplitudes: $\langle a_n^2\rangle = \langle(a_n - \langle a_n\rangle)^2\rangle$. It takes ~10 min (~1200 contours) to acquire a sufficient amount of data for statistical analysis of the membrane fluctuations (examples of fluctuation spectra are given further below (see, e.g., Fig. 5 *A*)). The amplitudes of the modes with odd values of n average out to zero for an up/down symmetric vesicles, which is the case for the prolate vesicles studied here. When the thermal fluctuations are small, the amplitudes have a Gaussian distribution (see, e.g., Fig. 6 *A*).

The fluctuation analysis was performed for vesicles, which had sedimented to the bottom of the chamber. Gravity is known to cause the vesicles to deform (49) affecting the first modes of the fluctuation spectra (35). The effect of gravity depends primarily on the dimensionless gravity parameter $g_0 = \Delta\rho g R^4/\kappa$ (49), where $\Delta\rho$ is the density difference (in our experiments $\Delta\rho \le 0.012$ g/cm^3) and g is the acceleration of gravity (in the lab). For a fixed density of the solution, larger vesicles deform more than smaller ones. Henriksen et al. (50) suggested a gravity criterion, which can be used to estimate the maximal size, R_{max}, of the vesicle below, of which the gravity effects are negligible. This maximal size is given by the implicit relation $g_0 = \Delta\rho g R_{max}^4/\kappa \le 12 + \sigma R_{max}^2/\kappa$ (50), where σ is the membrane tension. In our experiments $\sigma \ge 2 \times 10^{-5}$ dyn/cm. For DOPC vesicles, the bending modulus is $\sim 5 \times 10^{-13}$ erg (51,52) and may even increase due to the adsorbed avidin (a similar protein, i.e., streptavidin, was shown to stiffen lipid membranes (53,54)). For vesicles of size below ~16 μm, the above gravity condition is satisfied. The vesicles selected for our analysis have radii between 9 and 16 μm, thus gravity should not have significant effect on our measurements.

The fluctuations of the a_n-modes contain the information about both the spontaneous curvature and the rigidity of the membrane (for every axisymmetrical shape such as the prolate, the amplitudes b_n in Eq. 2 are zero). The membrane spontaneous curvature, M_{sp}, is proportional to the ratio of the mean-square average values of the second and the third modes (34):

$$M_{sp} \propto \langle a_3^2\rangle/\langle a_2^2\rangle \equiv \bar{M}_{sp}. \tag{3}$$

This dimensionless curvature ratio, $\bar{M}_{sp}$, is determined directly from the experimental data. One way to estimate the absolute value of the spontaneous curvature, M_{sp}, is to match the experimentally measured fluctuations with a spectrum generated by Monte Carlo simulations (16,55). An alternative method is to use the discretization of the spontaneous curvature reported in the literature (34,35), where analytical expressions for a_2 and a_4 as functions of the spontaneous curvature and the reduced volume, v, are given. Unfortunately, with this latter approach the effective spontaneous curvature cannot be determined very precisely, due to large experimental and numerical errors, especially for vesicles with a relatively large reduced volume v close to unity (in our measurements, we typically had $v \ge 0.9$). In this study we did not attempt to estimate the absolute value of the spontaneous curvature but the change induced by anchoring the polymers. Thus, we will analyze the data to determine the change in the curvature ratio $\bar{M}_{sp}$.

We used vesicles whose fluctuation spectrum was stable within at least ~1 h before introducing the DNA and was then not affected during the shear stress test (see Setup and Experimental Steps). The data collected during these first two phases were used to determine the error of the measurement. All vesicles were prolates with an initial curvature ratio $\bar{M}_{sp} = \bar{M}_{sp}^{in}$ between 0.238 ± 0.047 and 1.141 ± 0.029. After DNA was introduced in the experimental cell, the measurements were continued until no further changes in the curvature were detected. Osmotic effects were ignored because the osmolarities of all the solutions were very carefully matched and no change in the vesicle volume was detected. We denote the curvature ratio after anchoring of polymers as $\bar{M}_{sp}^{fi}$. The net effect from attaching the DNA is then expressed as the difference $\Delta\bar{M}_{sp} = \bar{M}_{sp}^{fi} - \bar{M}_{sp}^{in}$. Because the initial state of every vesicle is different, i.e., different $\bar{M}_{sp}^{in}$ and v, we use $\Delta\bar{M}_{sp}$ (instead of directly comparing $\bar{M}_{sp}^{fi}$) to compare the changes in the spontaneous curvatures measured on different vesicles.

The bending stiffness, κ, on the other hand is inversely proportional to the membrane fluctuations, $\kappa \propto k_BT/\langle a_n^2\rangle$, where k_BT is the thermal energy (35). The actual bending elasticity modulus of the decorated membrane can be estimated when the measured fluctuation spectra are matched to spectra generated with Monte Carlo simulations (16,56). The simulations use the full Hamiltonian of the area-difference elasticity model and take into account the contribution of the gravitational forces acting on the vesicle. Here and below, we discuss only the qualitative effect of the anchored polymers on the membrane stiffness. Roughly, the membrane fluctuations can be expressed as (56,57)

$$\langle a_n^2\rangle = (k_BT/\kappa)\{(n+2)(n-1)[n(n+1)-w']\}^{-1}, \quad (4)$$

where w' is a function of the spontaneous curvature and the dimensionless Lagrange multiplier.

Vesicle morphology and trajectories in the shape phase diagram

According to the area-difference elasticity model (35,58), which applies to lipid bilayers with no flip-flop between the two monolayers, the shape of a vesicle is uniquely determined by the vesicle reduced volume and the effective reduced area difference. The latter consists of two components: the ''local'' spontaneous curvature and the global difference in the area of the two leaflets. In the experimental conditions of this study, no exchange between the two leaflets is expected on the timescale of the experiment, suggesting that their areas remain fixed (the adsorbed avidin and the bound DNA were not expected to flip-flop because of the relatively large size of these molecules; see Fig. 1 *B*). Thus the change in the location of the vesicle in the morphological diagram would be determined mainly by the membrane spontaneous curvature M_{sp} and the vesicle reduced volume v. The knowledge about the initial state of the vesicle and its trajectory is important for comparing the DNA-induced effect because different vesicles do not have identical morphology.

During an experiment, the vesicle can follow different trajectories depending on the initial shape and the changes in the reduced volume v and spontaneous curvature M_{sp} as induced by the anchored polymer. To illustrate this point, we consider a fraction of the morphological diagram (which depends on v and M_{sp} only; see Fig. 3), corresponding to cases experimentally relevant for this work. We consider the range where the reduced volume v is above 0.9 because, for the vesicles presented here, v varied between 0.91 and 1. Defect-free vesicles with smaller v were not found in the solution even though we attempted to deflate the vesicles osmotically. A possible reason for the absence of such vesicles could be the modified membrane properties due to the adsorbed avidin. All vesicles observed in this study initially had prolate shapes (the fluctuation spectra of >60 vesicles were measured, data not shown) and, therefore, were located above the metastability line for oblate-prolate transition, and below the prolate/pear transition line (see Fig. 3). As discussed above, the grafted polymers are expected to increase the membrane spontaneous curvature ($\Delta M_{sp} > 0$), equivalent to moving the vesicle shape upwards in the morphological diagram. During the experiments, the enclosed vesicle volume remains constant because of the osmotic stabilization. On the other hand, the grafting of polymers on the external leaflet of the vesicle membrane is expected to reduce the projected vesicle area (as optically detected) by locally pulling on the membrane (17–19). As a result, the value of the reduced volume can only increase or remain constant within the experimental error of the measurement ($\Delta v \geq 0$), and the vesicle can slightly shift to the right in the morphological diagram (see trajectory *1* in Fig. 3). Thus, by monitoring the changes in the vesicle reduced volume and spontaneous curvature, one can determine the trajectory in the morphological diagram.

Budding transition

The fluctuation analysis described above is applicable only to prolate vesicles, i.e., vesicles located between the spinodals of oblate/prolate and the pear/bud transitions (see Fig. 3). As we will see further below, when the DNA solution is introduced, vesicles with a certain anchor concentration undergo a budding transition. Budding is a shape transformation where the vesicle expels a small satellite vesicle or bud connected to the initial vesicle via a thin neck. During budding, the vesicle exhibits large shape fluctuations and crosses the pear/prolate phase transition line (see Fig. 3). In these cases, because the vesicle shape exhibits broken up-down symmetry, the change in membrane spontaneous curvature induced by the polymer cannot be obtained by fluctuation spectroscopy. Instead, the size of the ''mother'' vesicle and the expelled bud were measured. Both of them have spherical topology and are connected by a thin neck, which is optically not resolvable. If the compositions of the mother vesicle (*M*) and the bud (*B*) are identical and homogeneous, the spontaneous curvature of the system is satisfied by the relation (3):

$$M_{sp}^{fi} = 1/2(M^M + M^B), \quad (5)$$

where M^M and M^B are the mean curvatures of the mother vesicle and the bud, respectively. The radii of the latter were estimated from the analysis of the video micrographs. The spontaneous curvature as estimated from Eq. 5 is a combination of the effect of anchored DNA and of the inherent spontaneous curvature of the selected vesicle. The initial spontaneous curvature M_{sp}^{in} of a giant unilamellar vesicle before budding is usually considered as being close to zero because the membrane is essentially flat on a microscopic level (~0.5 μm). Hence, we assume that the initial spontaneous curvature of the vesicle before budding is negligible compared to the effect arising from the insertion and anchoring of the DNA: $\Delta M_{sp} = M_{sp}^{fi} - M_{sp}^{in} \approx M_{sp}^{fi}$. The quantity ΔM_{sp} is in units [μm^{-1}] and cannot be directly compared with the dimensionless curvature ratio $\Delta\bar{M}_{sp}$ measured from the fluctuation analysis.

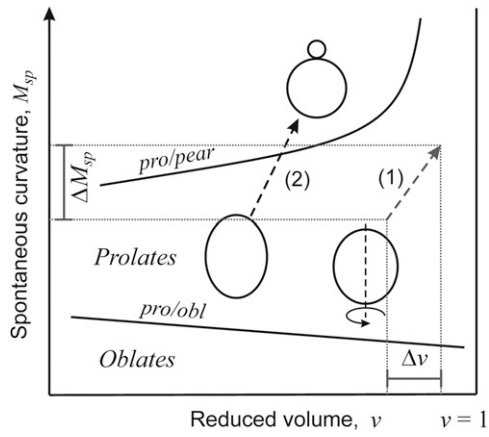

FIGURE 3 Schematic presentation of the morphological diagram illustrating the trends in the vesicle shape transformation as a function of reduced volume, v, and spontaneous curvature, M_{sp} (reproduced from (35)). The range of reduced volumes covered on the abscissa is between ~0.9 and 1. The trajectory indicated with (1) represents a prolate vesicle whose spontaneous curvature increases by ΔM_{sp} and whose reduced volume increases by Δv (the change in v is exaggerated for clarity). When the induced ΔM_{sp} is large, the vesicle can cross the prolate/pear instability line and undergo a budding transition as happens for trajectory (2).

EXPERIMENTAL RESULTS

Surface concentration of anchors

When anchored to one side of a planar membrane, the configurational entropy of a polymer chain increases if the membrane bends away from it. Thus, anchored polymers exert

entropic force onto the bilayer and the membrane attains a certain spontaneous curvature (17). The magnitude of this effect is governed by the polymer surface concentration, Γ, defined as the number of polymers per unit area. Depending on Γ, one distinguishes two regimes in the behavior of the polymer-induced curvature: 1), mushroom; and 2), brush regime (18,19). For low coverage, i.e., small Γ, corresponding to the mushroom regime, the average distance between the polymers is much larger than their size. For high coverage corresponding to the brush regime, the macromolecules are densely packed leading to constraints on the polymer configurational entropy arising from the confinement by the neighboring chains. The overlap concentration separating the two regimes is referred to as overlap (ov) concentration $\Gamma^{ov} = 1/\pi R_p^2$. At this coverage, the distance between the polymers is comparable to the radius of the polymer coil. In this work, we studied surface concentrations, which belong to the mushroom regime.

The characteristic dimension of a polymer in solution is given by its end-to-end distance, R_p, which is related to the mean-square distance between the first and the last segment. For an ideal or Gaussian polymer chain (as appropriate for a polymer in a θ-solvent), one has $R_p = a_p\sqrt{N}$, where a_p is the persistence length of the polymer, and N is the number of statistically independent polymer segments. The λ-phage DNA has 48,502 basepairs and the number of independent segments is $N = 170$; the polymer persistence length is $a_p =$ 50 nm, which implies an end-to-end distance $R_p = 0.65\ \mu$m (59,60).

By following the protocol outlined in Setup and Experimental Steps, several different concentrations of avidin anchors, Γ_{an}, on the vesicle surface were studied, where Γ_{an} is the surface concentration of biotinylated lipids in the external monolayer of the vesicle membrane. To facilitate the presentation of the experimental data the anchor concentrations will be given as fractions of the overlapping concentration Γ^{ov}. For our system, i.e., when the polymer is λ-phage DNA, $\Gamma^{ov} \cong 0.75\ \mu m^{-2}$. The range of surface concentrations Γ_{an} that can be experimentally studied is limited by two factors. First, the lowest physically achievable concentration corresponds to one anchor per vesicle. Taking 10 μm as a typical vesicle radius, one obtains $\sim$0.001 Γ^{ov} for the lowest possible Γ_{an}. The upper limit for Γ_{an} is set by Γ^{ov}: increasing the surface concentrations of anchored polymers above Γ^{ov} would lead to a dense coverage and the membrane of the vesicle would, presumably, no longer be accessible for the binding of new polymers. As it will be demonstrated further below, this exclusion effect is exhibited already at anchor concentrations of $\sim$0.3 Γ^{ov}.

As explained in Materials, Methods, and Experimental Procedure and Fig. 1, the biotinylated DNA is attached to the biotin-lipid anchors via avidin linkers. Therefore, the concentration of anchored DNA, Γ, may differ from the anchor concentration Γ_{an}. However, the working concentration of biotin-lipid anchors is extremely low while the avidin in the solution is in large excess, implying that every biotinylated lipid binds to one avidin. On the other hand, the DNA is much larger than the avidin anchor. Thus, it is reasonable to assume that only one DNA binds to one avidin anchor. The anchor concentrations we have explored are in the very dilute regime while the DNA is always in excess; thus, we expect that all of the sites be occupied.

We attempted to measure the concentration of the anchored DNA polymers from the fluorescence signal detected with confocal microscopy but quantification was not possible due to fast bleaching of the dye (recently we realized that the fluorescent dye YOYO-1, from Molecular Probes, is more suitable for such measurements in terms of stability; however, this molecule was not available to us during the performed experiments). The observations only confirmed that the biotinylated DNA attaches to the vesicles since we detected fluorescence signal from the vesicle surface. The nonbiotinylated DNA, on the other hand, did not attach to the membrane since no fluorescence was detected from the vesicle surface. Fig. 4 presents two examples of images recorded from two vesicles at anchor concentrations 0.12 Γ^{ov} and 0.6 Γ^{ov}. To facilitate the scanning and to avoid interference of signal from the displacement of the vesicles, the latter were immobilized on the wall of the observation chamber. In the latter case, the chamber interior was not coated by albumin, an essential procedure for all other cases (see Setup and Experimental Steps). The fluorescence intensity from the

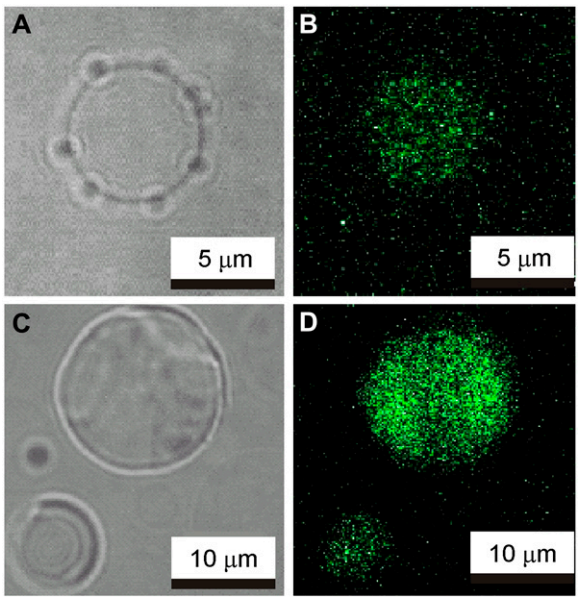

FIGURE 4 Vesicles immobilized on glass surface in the presence of fluorescently labeled DNA. The anchor concentrations are 0.12 Γ^{ov} in panels *A* and *B* and 0.6 Γ^{ov} in panels *C* and *D*, with Γ^{ov} being the overlap concentration. In panels *A* and *B*, the vesicles are observed in transmitted light with a 100× oil immersion objective. The images in panels *C* and *D* show the fluorescence signal from the same two vesicles. Both micrographs have been enhanced by duplicating the signal from all color channels.

vesicle with higher anchor concentration appears to be higher, but exact quantification of the signal was not possible as the intensity depends on the vesicle radius, the scanning and exposure time, dye bleaching, etc. For these two images, we attempted to apply similar scanning conditions. Further in the text, we compare the results for different coverage concentrations with respect to the surface concentration Γ_{an}.

Each experiment for a particular value of Γ_{an}, as described in Setup and Experimental Steps, consists of the following steps:

1. Selection of a suitable vesicle.
2. Testing the stability of the fluctuation spectrum.
3. Shear stress and adhesion test performed by flushing buffer in the chamber.
4. Measurements of the fluctuation spectrum after introducing the DNA solution.

In all the experiments, the amount of DNA flown in the chamber was always the same and in excess compared to the total concentration of avidin anchors. Thus, we expect that the surface concentration of anchored polymers depends uniquely on the concentration of avidin anchors Γ_{an}. Two types of vesicle response were observed depending on the value of Γ_{an}. At low surface concentration of anchors, a change in the fluctuation spectrum was detected. The curvature ratio $\bar{M}_{sp}$ was extracted from the measured spectra (see Eq. 3). At high Γ_{an}, the vesicles underwent budding transitions and ΔM_{sp} was estimated from the size of the bud and the mother vesicle (see Eq. 5). For vesicles with intermediate concentration of anchors, both types of behavior were observed and both approaches to estimate the change in the spontaneous curvature were applied.

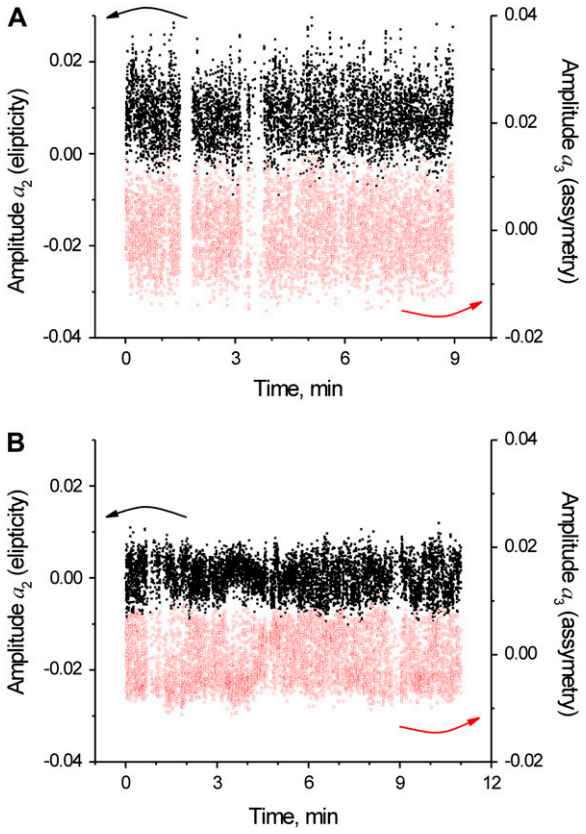

FIGURE 5 Time series of the mode amplitudes a_2 (*solid squares*, *left axes*) and a_3 (*open squares*, *right axes*), for a vesicle with equivalent sphere radius $R_0 = 9$ μm. The anchor concentration has the value of 0.06 Γ^{ov}. Panels *A* and *B* correspond to the time evolution before and after introducing the DNA solution in the chamber, respectively. Due to the anchored DNA, the membrane fluctuations decrease (to facilitate the comparison, the vertical axes of both graphs have the same scale).

Vesicle response at low anchor concentration

We start with an example where the effect on the vesicle spontaneous curvature was determined from fluctuation analysis. Fig. 5 presents the time series of the modes a_2 and a_3 for a vesicle with anchor concentration $\Gamma_{an} = 0.06\ \Gamma^{ov}$. Such coverage corresponds to 1 anchor per $\sim 20\ \mu m^2$ vesicle surface. The vesicle size is $R_0 = 9\ \mu$m (effectively only ~ 45 polymers could be anchored to this vesicle at this Γ_{an}). The initial reduced volume of the vesicle was $v = 0.992$. Fig. 5 *A* presents data obtained when the vesicle fluctuation spectrum was examined for stability. Similar time series were recorded after applying shear stress by flushing buffer in the chamber whereby the vesicle fluctuation spectra remained the same with respect to the mean values and mean-square amplitudes of the modes (data not shown). The data presented in Fig. 5 *B* were collected some time after the DNA was introduced in the chamber. The change due to anchored polymers is encoded in the decrease of the vesicle ellipticity, $\langle a_2 \rangle$. The average value of a_3 (vesicle asymmetry) remains unaffected and close to zero. A pronounced decrease in the membrane fluctuations for both modes was detected and will be discussed further in the text. Similar trend was observed for the higher modes. The distribution histograms of a_2 and a_3 before and after anchoring the polymers are presented in Fig. 6. When the thermal fluctuations are small they can be considered as Gaussian, confirmed by the goodness of the fits on the figure. The amplitude distribution for the vesicle with anchored polymers is much narrower than the corresponding one for the same vesicle without anchored polymers.

Before we continue with the results on the change in the spontaneous curvature as a function of the concentration of anchored polymers, we discuss the following test experiment. The latter was aimed to account for possible effect due to an asymmetry of the solutions across the membrane or entropic pressure exerted by the nonanchored macromolecules. For this purpose we flushed nonbiotinylated DNA in the working chamber. Such DNA is deprived of the possibility to attach to the membrane because it does not have the anchoring group (biotin). The effect on the fluctuation spectra could not be distinguished from the effect of the simple shear stress test mentioned above. Therefore no measurable influence can be expected from the nonanchored

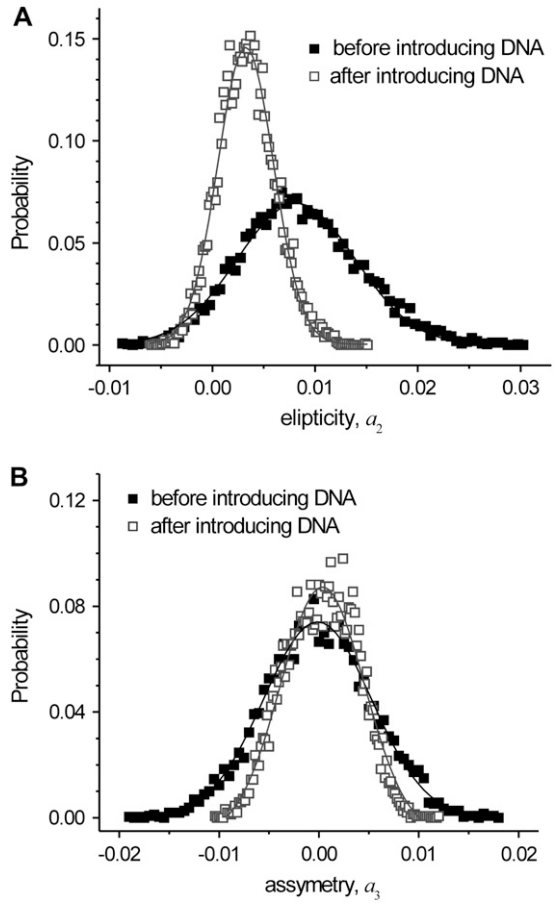

FIGURE 6 Normalized histograms for the mode amplitudes a_2 and a_3, based on the time series presented in Fig. 5. The surface concentration of the biotin anchors has the value of $\Gamma_{an} = 0.06\ \Gamma^{ov}$. Two sets of data are shown corresponding to before (*solid squares*) flushing DNA into the chamber and after (*open squares*) introducing DNA. When the membranes are decorated with DNA, the distributions become narrower, indicating a drop in $\langle a_n^2 \rangle$. The solid lines are Gaussian fits to the data.

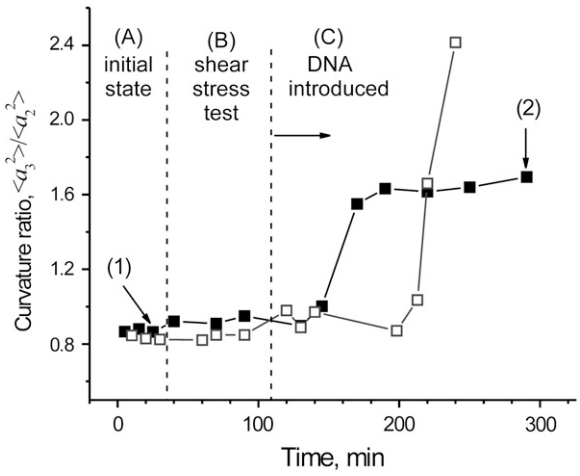

FIGURE 7 Time evolution of the curvature ratio for two vesicles that differ in the surface concentration of anchors, Γ_{an}. The solid and the open squares correspond to $\Gamma_{an} = 0.06\ \Gamma^{ov}$ and $0.3\ \Gamma^{ov}$, respectively. Each point represents an average over 10 min of data acquisition. The data points indicated as (1) and (2) correspond to the measurements from Fig. 6. The dashed lines separate the three phases of the experiment: (*A*) test of fluctuation spectrum stability, (*B*) shear stress test by flushing buffer into the chamber, and (*C*) introducing DNA solution (see Budding Transition for details). The reduced volume, v, of the vesicle with anchor concentration $0.3\ \Gamma^{ov}$ reaches $v = 1$ in phase *C*, after which no fluctuations are observed.

polymers. In addition, it suggests that no effect is detected if the polymer only adsorbs but does not anchor on the vesicle surface.

To illustrate the change in the membrane spontaneous curvature induced by the anchored DNA molecules in Fig. 7 we present the time evolution of the curvature ratio $\langle a_3^2 \rangle / \langle a_2^2 \rangle$. The two data sets are from the full experiments (here with ''experiment'' we denote a set of measurements of the fluctuation spectra of one vesicle) with two different vesicles of anchor concentrations $\Gamma_{an} = 0.06\ \Gamma^{ov}$ and $\Gamma_{an} = 0.3\ \Gamma^{ov}$, i.e., 1 anchor per 20 μm^2 and 5.5 μm^2 of vesicle surface, respectively. Each data point on Fig. 7 represents a 10-min measurement of the membrane fluctuation spectrum and the data points indicated as (1) and (2) were obtained from those presented in the data sets in Figs. 5 and 6. The three phases of the experimental procedure (Setup and Experimental Steps) are separated by vertical dashed lines. Obviously, flushing the buffer solution (''shear stress test'' or phase B) does not have a measurable influence on the fluctuation spectrum (compare phases A and B). The data from these two phases provide an estimate of the error of the measurement introduced by shearing the vesicle. In contrast, introducing the DNA solution leads to a dramatic change in the curvature ratio.

Intermediate anchor concentration

The change in the curvature ratio is more pronounced for higher anchor concentration. It is important to remember that the value of $\bar{M}_{sp}^{in}$ for each individual vesicle is different. For simplicity, in Fig. 7 we have presented data for two vesicles with similar $\bar{M}_{sp}^{in}$ to demonstrate the larger increase in the curvature ratio for the higher anchor concentration. In fact, the curvature ratio for the vesicle with $\Gamma_{an} = 0.3\ \Gamma^{ov}$ does not reach saturation. The vesicle with $\Gamma_{an} = 0.3\ \Gamma^{ov}$ is actually in the anchor concentration regime where both budding and fluctuation analysis were applied. The vesicle spheres and the thermal fluctuations vanish, making the fluctuation analyses inapplicable. This is due to a decrease in the area available for fluctuations (the optically resolved area of the vesicle obtained from contour analysis is observed to decrease). On the other hand, as mentioned before, the enclosed vesicle volume remains constant due to osmotic stabilization. Thus, the reduced volume, v, increases and the vesicle follows trajectory *1* in the phase shape diagram in Fig. 3. In this particular case v reaches 1, i.e., the vesicle becomes spherical. A plausible explanation for the decrease in the area available for fluctuations is that, when anchored, the polymers

locally pull at the membrane, creating tiny cones which are optically irresolvable (below ~0.5 μm in height) but effectively reduce the area available for fluctuations. Perturbative calculations and Monte Carlo simulations (19) have shown that close to the anchor the membrane bends away from the anchored polymer and attains conical shape. Knowing the geometrical shapes of the cones and the number of anchored polymers would then allow for an estimate of the area hidden in the cones. However, the theoretical calculations were performed for flexible polymer while, in our case, the DNA molecule having a persistence length of 50 nm should be considered instead as a semiflexible polymer. We also do not exclude the possibility that the vesicle has undergone budding transition with bud size below optical resolution, which would also lead to effective loss of area. This would be consistent with the longer time the vesicle needed to respond as compared to the one with lower anchor concentration. The budding transition involves overcoming an energy barrier, and thus can occur later.

Another factor that has to be considered when the vesicle spheres up is the membrane tension. Typical tensions of floppy vesicles are in the range of $\sigma \sim 10^{-5}$–10^{-4} dyn/cm. The vesicle loses area due to the anchored polymer. Because the volume stays constant, the membrane tension can increase (particularly for vesicles of reduced volume close to unity), and in this way, impose constraints on fluctuations of larger wavelengths (smaller modes). Thus, the interpretation of data from vesicles, which have reached $v \approx 1$, is more complex because the membrane tension has increased and the fluctuation spectra of such vesicles would give lower values for $\langle a_n^2 \rangle$ at small n, and respectively influence the value for the curvature ratio.

Coming back to Fig. 7, it is interesting to note that the increase in the curvature ratio was not observed immediately after DNA was introduced in the microchamber (the complete exchange of the chamber solution with the DNA solution would typically take ~4–5 min). Considering the low diffusion coefficient of the DNA molecules (0.47 ± 0.03 $\mu m^2/s$ (61)), one can speculate that the delay in the effect on the membrane curvature is due to the time the biotinylated end of a DNA molecule needs to locate an avidin anchor on the membrane. In the different experiments, this time has varied between 20 min and 80 min slightly, depending on the anchor concentration on the membrane. The difference in time for the response of the two vesicles in Fig. 7 is also due to the different location of the vesicles in the experimental chamber. While the one with lower anchor concentration was located close to the injection port for introducing the DNA solution in the chamber (see Fig. 2), the other one was far. To avoid losing the vesicle from the chamber a lower flow rate of the injected DNA solution was used (the injection of the whole volume of the DNA solution took ~20 min), which involved a longer time for the vesicle response.

The completion of the anchoring process usually results in reaching a plateau in the curvature ratio. We assume that equilibrium has been reached if the curvature ratio remains constant within a time interval larger than ~2 h after the increase has been observed (the vesicle with $\Gamma_{an} = 0.3\ \Gamma^{ov}$ in Fig. 7 falls out of this category because it sphered up). Further in the text, as a final value for the ratio $\langle a_3^2 \rangle / \langle a_2^2 \rangle$ we have taken the saturation value. In the experiment at $\Gamma_{an} = 0.06\ \Gamma^{ov}$, for the initial and final curvature ratio we obtained $\bar{M}_{sp}^{in} = 0.866$, $\bar{M}_{sp}^{fi} = 1.695$.

Expected dependence of the spontaneous curvature on the anchor concentration

Before we continue with higher surface concentrations at which vesicles undergo budding transition, we consider again the observed overall drop in the vesicle fluctuations. This decrease is expected for two reasons:

1. When anchored to the membrane, the polymers pull at the membrane (17,19), thus reducing the free area otherwise available for fluctuations. This effect is expressed in an increase in the reduced volume, directly accessible and observed from the fluctuation analysis data.
2. The mean-square averages of the amplitudes of the fluctuation spectrum are inversely proportional to the bending stiffness, which is expected to increase (17,18).

The change in the membrane curvature and the elastic properties as induced by anchored polymers in the different regimes has been determined theoretically using scaling arguments, analytical calculations for ideal chains, and Monte Carlo simulations (17–19,24). As a result, one finds that the membrane always bends away from the polymer, and the membrane spontaneous curvature behaves as

$$M_{sp} \approx \sqrt{\pi/6}\,(k_B T/4\kappa) R_p \Gamma + (A_{an}/2l_{me})\Gamma + b_2 (k_B T/4\kappa) R_p \Gamma^2, \quad (6)$$

for small surface concentration Γ, where A_{an} is the surface area occupied by the anchor, l_{me} is the membrane thickness ($l_{me} \cong 4$ nm), and b_2 is the second virial coefficient, $b_2 = 4\pi R_p^2$. The first term in Eq. 6 arises from the polymer/membrane interactions while the second accounts for the contribution of the polymer anchor to the monolayer area (the term is valid for conditions of no flip-flop between the two bilayer leaflets). The third term in Eq. 6 reflects possible polymer/polymer interactions as, because the lipid membrane is fluid, the anchored polymers can diffuse and occasionally collide. The anchor contribution (second term) is usually small if the anchor is a lipid whose headgroup ($A_{an} \cong 0.7\ nm^2$) is covalently bound to the polymer (the effect of the anchor characteristics was studied in detail in (62)).

Equation 6 predicts that the dependence of the spontaneous curvature is linear in Γ for low mushroom concentrations, but quadratic for higher concentrations. One can define a crossover surface concentration, Γ^*, above which the polymer/polymer interactions arising from the excluded volume

become dominant over the entropically induced polymer/membrane interactions. Assuming that the anchor contribution (second term in Eq. 6) is small, $\Gamma*$ can be estimated by equating the spontaneous curvatures from the first and the third term in Eq. 6. One obtains

$$\Gamma* = 1/4\sqrt{6\pi}R_p^2 \simeq 0.18\,\Gamma^{ov}, \quad (7)$$

which is somewhat smaller than Γ^{ov}.

Dependence of the bending stiffness on the anchor concentration

The overall bending stiffness of the membrane is expected to increase due to the anchored polymers yielding an effective bending stiffness (18),

$$\kappa_{eff} \approx \kappa + c_\kappa\,\Gamma R_p^2 k_B T, \quad (8)$$

with $c_\kappa = 1/12(1+\pi/2)$. Equation 8 reduces to $\kappa_{eff} \approx \kappa + 0.068\,k_BT$ at the overlap concentration ($\Gamma = \Gamma^{ov}$). The linear increase of the bending stiffness as a function of the polymer surface concentration was recently confirmed for microemulsion droplets stabilized by a surfactant layer and anchored diblock copolymers (23). However, the dimensionless coefficient c_κ was found to be a factor of 1.5 larger than the theoretical results for ideal chains and was ascribed to the polymer properties and deviation from θ-solvent conditions.

As demonstrated in the literature (35,63), the mean-square average of the fluctuation modes is inversely proportional to the bending modulus of the membrane (see Eq. 4). Therefore, the overall reduction in the membrane fluctuations can imply an increase in the bending stiffness of the membrane. Indeed, an overall decrease in the mean-square values of the modes is observed. Fig. 8 presents the mean-square averages of the first 20 amplitudes of the vesicle spectra before and after flushing the buffer and also after introducing the DNA solution. The buffer does not change significantly the values of $\langle a_n^2 \rangle$, but the anchoring of the polymers decreases them. The dashed lines show fits according to Eq. 4 where κ and w' were used as fitting parameters. In absence of DNA, we obtain $\kappa = 22.2 \pm 1.7\,k_BT$ and $w' = 16.3 \pm 1.8$. Anchoring of the DNA leads to $\kappa = 32.1 \pm 8.0\,k_BT$ and $w' = 288.7 \pm 78.6$. The relatively large scatter of the data does not allow for precise comparison, but it is clearly seen that the bending stiffness of the membrane increases.

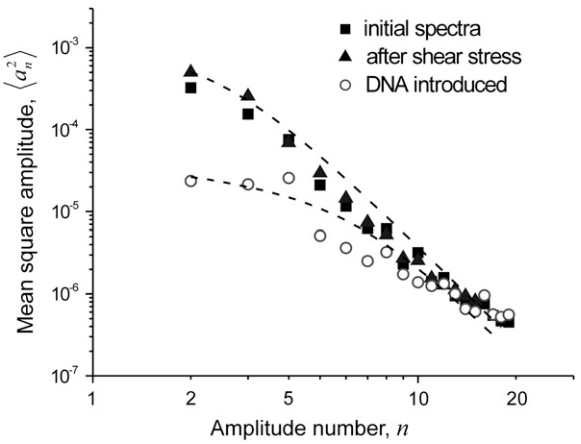

FIGURE 8 Mean-square amplitudes for three different 10-min measurements: initial fluctuation spectra, shear stress test, and after introducing DNA. The surface concentration of anchors is 0.03 Γ^{ov}. The first amplitude cannot be distinguished from zero and is not shown. The dashed lines are fits according to Eq. 4 (see text for details).

High anchor concentration (vesicle budding)

As mentioned before, at high coverage ($\Gamma_{an} \geq 0.12\ \Gamma^{ov}$) budding transitions were observed. In some cases multiple budding was observed whereby a necklace of interconnected vesicle pearls was gradually formed (see Fig. 9). The pearls do not have identical sizes. The diameter of the bud formed first is ~4.1 μm, while the rest of the pearls have approximately equal and smaller diameters (~1.4 μm). A plausible reason for the different diameters could be that the individual vesicle pearls have a different number of anchored polymers (each of the small pearls should have approximately four anchors if the anchor concentration is homogeneous). The change in the membrane spontaneous curvature was estimated by analysis of the bud size (see Budding Transition). It is important to note that Eq. 5 is valid if the mother vesicle and the buds have the same composition. In attempt to clarify whether the anchor distribution was homogeneous, we performed tests about the miscibility of the lipids DOPC and biotinyl-Cap-PE using differential scanning calorimetry on extruded unilamellar vesicles. No phase separation was observed for the lipid molar ratios used in this work, suggesting that the anchors were homogeneously distributed on the vesicle surface. The attached avidin is also not expected to induce phase separation, as suggested by previous studies performed at higher avidin concentrations (54). This, of course, does not rule out the possibility that when anchored to the membrane the DNA molecules aggregate in clusters or domains, thus creating inhomogeneity in the polymer surface concentration. In this case, to extract the spontaneous curvature one has to take into account the line tension of the domain edge (3,64,65). Effects of coupling of the local curvature and polymer concentration were observed experimentally on tubular vesicles (29), and theoretically addressed (66,67). Here, the composition of the vesicles was assumed to be homogeneous due to the very low surface concentration of the polymer.

Overall concentration dependence of the spontaneous curvature (summary)

A summary of all the data on the spontaneous curvature as a function of anchor concentration is given in Fig. 10, where the results obtained from both fluctuation and bud size

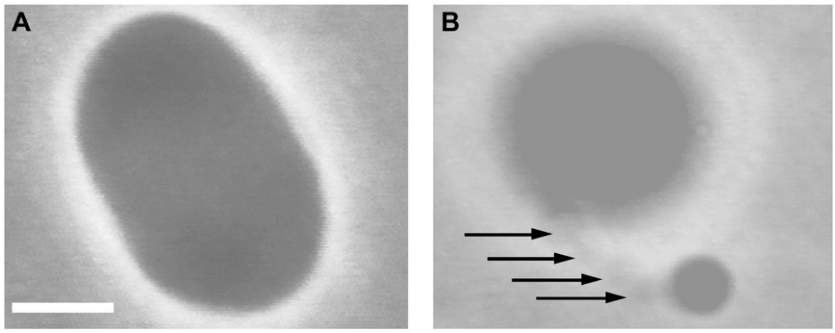

FIGURE 9 (*A*) A vesicle with surface coverage $\Gamma^{an} = 0.3\ \Gamma^{ov}$ and reduced volume $v = 0.975$. The scale bar corresponds to 5 μm. (*B*) Multiple budding observed after the DNA solution is introduced. The bud formed first (diameter $\approx 4.1\ \mu$m) is connected to the ''mother'' vesicle (diameter $\approx 12.7\ \mu$m) with a necklace of vesicle pearls (diameters $\approx 1.4\ \mu$m). The necklace and the mother vesicle are out of focus but the pearl locations are shown with arrows.

analysis are presented. The figure contains data from 20 vesicles altogether and the error bars indicate averaging over approximately three vesicles. In the low surface concentration limit one observes a gradual linearlike increase in the spontaneous curvature ratio. In two of the cases (*open symbols*), no saturation in the curvature ratio could be observed because the vesicles attained spherical shape. The linear increase in the spontaneous curvature is consistent with the theoretical expectations for mushroom regime (see Eq. 6). Above $\Gamma_{an} = 0.12\ \Gamma^{ov}$ budding is observed and the analysis of the bud and mother vesicle size give the spontaneous curvature of the membrane. The latter is observed to be essentially constant, implying a constant surface concentration of anchored polymers. One possible explanation for this effect is the presence of packing constraints, arising from the nonideality of the polymer. Although the ions from the working buffer are expected to screen the negative charges along the DNA backbone and the net positive charge of the avidin, the presence of small uncompensated charges cannot be excluded. In the case of such unspecific electrostatic DNA-avidin attraction one can speculate that when anchored, the polymer will slightly spread over the membrane, covering a larger area than expected. Thus, the area between the anchored polymers accessible for new DNA would decrease and, for the free polymers in the solution, it will be entropically unfavorable to enter in the gaps between the anchored polymers (18). Thus, due to packing constraints above certain ''critical'' polymer coverage, the number of anchored polymers per unit area cannot increase even though the number of avidin anchors increases.

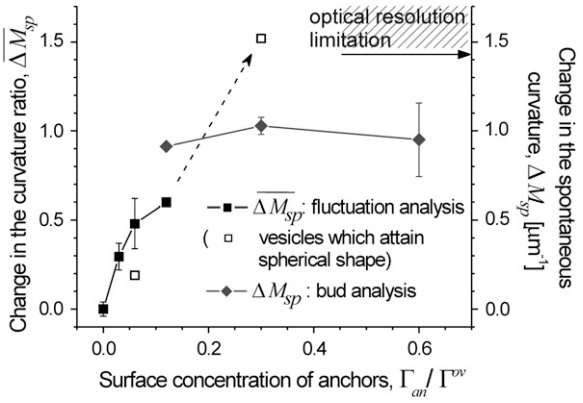

FIGURE 10 Effect of polymer grafting on the membrane: spontaneous curvature as a function of surface concentrations in the mushroom regime as obtained from fluctuation spectroscopy (*solid* and *open squares*), left axis, and bud analyses (*diamonds*), right axis. The open-square symbols indicate two cases when the vesicle attained a spherical shape and no saturation in the curvature ratio could be observed. Error bars indicate scattering over several vesicles. The optical resolution limit for bud detecting is indicated by the arrow.

The data in Fig. 10 imply that the absolute values of the polymer-induced curvature as obtained from the bud analysis are of the order of 1 μm^{-1} (43) whereas the theoretically expected ones for the mushroom regime are of the order of 10^{-3}–$10^{-2}\ \mu$m^{-1} (18,19). A few possible reasons can be considered to explain the discrepancy. One of them concerns the possibility of a nonuniform distribution of the anchored DNA as discussed above. The other one, which we favor more, relates to the fact that due to optical limitation, buds of radius below $\sim 1\ \mu$m could not be observed and, therefore, the experimental resolution imposes an upper limit to the value of the spontaneous curvature as measured from bud analysis (this is schematically indicated in Fig. 10). If present, such buds will suggest even larger spontaneous curvature. Furthermore, one should not forget that the predicted behavior of the spontaneous curvature was calculated for flexible polymer chains while the experiments described here were performed with semiflexible polymers. For flexible polymer chains, the induced curvature is predicted to depend only on the end-to-end distance R_p. For semiflexible chains, with persistence length a_p that is much larger than the membrane thickness, this curvature may also depend on these latter length scales.

CONCLUDING REMARKS

In this work, we characterized the membrane spontaneous curvature induced by anchoring of the biopolymer λ-phage DNA. A range of polymer surface concentrations in the mushroom regime was explored. Two approaches were applied for assessing the membrane spontaneous curvature: fluctuation spectroscopy for the low concentration region

and bud-size analysis for higher concentrations. We varied the number of anchors on the membrane surface, assessed the spontaneous curvature, and discussed the obtained experimental data in relation to existing theoretical expectations. In the low surface concentration limit, a gradual linearlike increase in the dimensionless spontaneous curvature ratio $\bar{M}_{sp}$ was observed. This linear behavior is consistent with theoretical expectations for flexible polymers (17–19). For the intermediate and high surface concentration, the membranes were observed to undergo budding shape transformations which are reminiscent of some theoretical (66,68) and experimental observations (28), and may be related to nonuniform surface concentration of the anchored polymers. Surprisingly, the spontaneous curvature obtained from the bud analysis is constant over a broad concentration range of the anchored polymers. We interpret this effect in terms of packing constraints arising from interactions between the polymers and the membrane, or reflecting the optical resolution limits. The induced spontaneous curvature, estimated from the bud analysis, is larger than the theoretically predicted one for the mushroom regime.

Although the membrane bending stiffness was not exactly determined in this work, we have some indications for membrane stiffening due to anchored polymers. Such effect was theoretically predicted (18) and experimentally confirmed for microemulsions (23).

Finally, using DNA as a model polymer has proved to be a suitable choice for mimicking biomolecular anchoring in cell membranes. To our knowledge, this study is the first to estimate the spontaneous curvature of membranes induced by anchored polymers.

We are grateful to H.-G. Döbereiner for providing the software for contour acquisition and fluctuation analysis, and for the many enlightening discussions. R. Georgieva is acknowledged for the help with the image acquisition using confocal microscopy.

REFERENCES

1. Bancroft, W., and C. Tucker. 1927. Gibbs on emulsification. *J. Phys. Chem.* 31:1681–1692.
2. Helfrich, W. 1973. Elastic properties of lipid bilayers: theory and possible experiments. *Z. Naturforsch.* 28:693–703.
3. Seifert, U., K. Berndl, and R. Lipowsky. 1991. Shape transformations of vesicles: phase diagram for spontaneous-curvature and bilayer-coupling models. *Phys. Rev. A.* 44:1182–1202.
4. Seifert, U. 1997. Configurations of fluid membranes and vesicles. *Adv. Phys.* 46:13–137.
5. Discher, B., Y.-Y. Won, D. Ege, J. Lee, F. Bates, D. Discher, and D. Hammer. 1999. Polymersomes: tough vesicles made from diblock copolymers. *Science.* 284:1143–1146.
6. Haluska, C. K., W. T. Góźdź, H.-G. Döbereiner, S. Förster, and G. Gompper. 2002. Giant hexagonal superstructures in diblock-copolymer membranes. *Phys. Rev. Lett.* 89:238302.
7. Keller, S. L., S. M. Bezrukov, S. M. Gruner, M. W. Tate, I. Vodyanoy, and V. A. Parsegian. 1993. Probability of alamethicin conductance states varies with nonlamellar tendency of bilayer phospholipids. *Biophys. J.* 65:23–27.
8. Lentz, B. R., D. P. Siegel, and V. Malinin. 2002. Filling potholes on the path to fusion pores. *Biophys. J.* 82:555–557.
9. Lipowsky, R., and E. Sackmann. Editors. 1995. Structure and Dynamics of Membranes. Elsevier Science, Amsterdam, The Netherlands.
10. Decher, G., E. Kuchinka, H. Ringsdorf, J. Venzmer, D. Bitter-Suermann, and C. Weisgerber. 1989. Interaction of amphiphilic molecules with model membranes. *Angew. Makromol. Chem.* 166:71–80.
11. Lipowsky, R., and H.-G. Döbereiner. 1998. Vesicles in contact with nanoparticles and colloids. *Europhys. Lett.* 43:219–225.
12. Döbereiner, H.-G., O. Selchow, and R. Lipowsky. 1999. Spontaneous curvature of fluid vesicles induced by trans-bilayer sugar asymmetry. *Eur. Biophys. J.* 28:174–178.
13. Dimova, R., S. Aranda, N. Bezlyepkina, V. Nikolov, K. A. Riske, and R. Lipowsky. 2006. A practical guide to giant vesicles. Probing the membrane nanoregime via optical microscopy. *J. Phys. Condens. Matter.* 18:S1151–S1176.
14. Lee, J. B., P. G. Petrov, and H.-G. Döbereiner. 1999. Curvature of zwitterionic membranes in transversal pH gradients. *Langmuir.* 15:8543–8546.
15. Petrov, P. G., J. B. Lee, and H.-G. Döbereiner. 1999. Coupling chemical reactions to membrane curvature: a photochemical morphology switch. *Europhys. Lett.* 48:435–441.
16. Döbereiner, H.-G., G. Gomper, C. K. Haluska, D. M. Kroll, P. G. Petrov, and K. Riske. 2003. Advanced flicker spectroscopy of fluid membranes. *Phys. Rev. Lett.* 91:048301.
17. Lipowsky, R. 1995. Bending of membranes by anchored polymers. *Europhys. Lett.* 30:197–202.
18. Hiergeist, C., and R. Lipowsky. 1996. Elastic properties of polymer-decorated membranes. *J. Phys. II France.* 6:1465–1481.
19. Breidenich, M., R. R. Netz, and R. Lipowsky. 2000. The shape of polymer-decorated membranes. *Europhys. Lett.* 49:431–437.
20. Bickel, T., C. Jeppesen, and C. M. Marques. 2001. Local entropic effects of polymers grafted to soft interfaces. *Eur. Phys. J. E.* 4:33–43.
21. Bickel, T., and C. M. Marques. 2002. Scale-dependent rigidity of polymer-ornamented membranes. *Eur. Phys. J. E.* 9:349–352.
22. Auth, T., and G. Gompper. 2003. Self-avoiding linear and star polymers anchored to membranes. *Phys. Rev. E.* 68:051801.
23. Gompper, G., H. Endo, M. Mihailescu, J. Allgaier, M. Monkenbusch, D. Richter, B. Jakobs, T. Sottmann, and R. Strey. 2001. Measuring bending rigidity and spatial renormalization in bicontinuous microemulsions. *Europhys. Lett.* 56:683–689.
24. Lipowsky, R. 2002. Domains and rafts in membranes—hidden dimensions of self-organization. *J. Biol. Phys.* 28:195–210.
25. Blume, G., and G. Cevc. 1990. Liposomes for the sustained drug release in vivo. *Biochim. Biophys. Acta.* 1029:91–97.
26. Ringsdorf, H., J. Venzmer, and F. M. Winnik. 1991. Interaction of hydrophobically modified poly-*n*-isopropylacrylamides with model membranes—or playing a molecular accordion. *Angew. Chem. Int. Ed. Engl.* 30:315–318.
27. Simon, J., M. Kfihner, H. Ringsdorf, and E. Sackmann. 1995. Polymer-induced shape changes and capping in giant liposomes. *Chem. Phys. Lipids.* 76:241–258.
28. Frette, V., I. Tsafir, M.-A. Guedeau-Boudeville, L. Jullien, D. Kandel, and J. Stavans. 1999. Coiling of cylindrical membrane stacks with anchored polymers. *Phys. Rev. Lett.* 83:2465–2468.
29. Tsafrir, I., D. Sagi, T. Arzi, M.-A. Guedeau-Boudeville, V. Frette, D. Kandel, and J. Stavans. 2001. Pearling instabilities of membrane tubes with anchored polymers. *Phys. Rev. Lett.* 86:1138–1141.
30. Lasic, D. D. Editor. 1993. Liposomes: From Physics to Applications. Elsevier Science Publishers, Amsterdam, The Netherlands.
31. Cates, M. E. 1991. Playing a molecular accordion. *Nature.* 351:102.
32. Evans, E., and W. Rawicz. 1997. Elasticity of ''fuzzy'' biomembranes. *Phys. Rev. Lett.* 79:2379–2382.

33. Marsh, D., R. Bartuccib, and L. Sportelli. 2003. Lipid membranes with grafted polymers: physicochemical aspects. *Biochim. Biophys. Acta.* 1615:33–59.

34. Döbereiner, H.-G. 1995. The budding transition of phospholipid vesicles: a quantitative study via phase contrast microscopy. Ph.D. Thesis, Simon Fraser University, Canada (unpublished).

35. Döbereiner, H.-G., E. Evans, M. Kraus, U. Seifert, and M. Wortis. 1997. Mapping vesicle shapes into the phase diagram: a comparison of experiment and theory. *Phys. Rev. E.* 55:4458–4474.

36. Rex, S., M. J. Zuckermann, M. Lafleur, and J. R. Silvius. 1998. Experimental and Monte Carlo simulation studies of the thermodynamics of polyethyleneglycol chains grafted to lipid bilayers. *Biophys. J.* 75:2900–2914.

37. Shivashankar, G. V., and A. Libchaber. 1997. Single DNA molecule grafting and manipulation using a combined atomic force microscope and an optical tweezer. *Appl. Phys. Lett.* 71:3727–3729.

38. Léger, J. F., G. Romano, A. Sarkar, J. Robert, L. Bourdieu, D. Chatenay, and J. F. Marko. 1999. Structural transitions of a twisted and stretched DNA molecule. *Phys. Rev. Lett.* 83:1066–1069.

39. Rye, H., J. M. Dabora, M. A. Quesada, R. A. Mathies, and A. N. Glazer. 1993. Fluorometric assay using dimeric dyes for double- and single-stranded DNA and RNA with picogram sensitivity. *Anal. Biochem.* 208:144–150.

40. Bordelon, J. A., K. J. Feierabend, S. A. Siddiqui, L. L. Wright, and J. T. Petty. 2002. Viscometry and atomic force microscopy studies of the interactions of a dimeric cyanine dye with DNA. *J. Phys. Chem. B.* 106:4838–4843.

41. Allemand, J. F., D. Bensimon, R. Lavery, and V. Croquette. 1998. Stretched and overwound DNA forms a Pauling-like structure with exposed bases. *Proc. Natl. Acad. Sci. USA.* 95:14152–14157.

42. Maier, B., and J. O. Rädler. 2000. DNA on fluid membranes: a model polymer in two dimensions. *Macromolecules.* 33:7185–7194.

43. Nikolov, V. K. 2004. Model membranes grafted with long polymers. Ph.D. Thesis, Potsdam University, Germany (unpublished).

44. Needham, D., and E. Evans. 1988. Structure and mechanical properties of giant lipid (DMPC) vesicle bilayers from 20°C below to 10°C above the liquid crystal-crystalline phase transition at 24°C. *Biochemistry.* 27:8261–8269.

45. Sanger, F., A. R. Coulson, G. F. Hong, D. F. Hill, and G. B. Petersen. 1982. Nucleotide sequence of bacteriophage λ-DNA. *J. Mol. Biol.* 162:729–773.

46. Schäfer, B., H. Gemeinhardt, V. Uhl, and K. O. Greulich. 2000. Single molecule DNA restriction analysis in the light microscope. *Single Mol.* 1:33–40.

47. Schäfer, B. 2001. Observations of structural changes and restriction analysis of single DNA molecules with fluorescent microscopy. PhD thesis, Friedrich-Schiller-Universität, Jena, Germany.

48. Yan, X., W. K. Grace, T. M. Yoshida, R. C. Habbersett, N. Velappan, J. H. Jett, R. A. Keller, and B. L. Marrone. 1999. Characteristics of different nucleic acid staining dyes for DNA fragment sizing by flow cytometry. *Anal. Chem.* 71:5470–5480.

49. Kraus, M., U. Seifert, and R. Lipowsky. 1995. Gravity-induced shape transformations of vesicles. *Europhys. Lett.* 32:431–436.

50. Henriksen, J. R., and J. H. Ipsen. 2002. Thermal undulations of quasi-spherical vesicles stabilized by gravity. *Eur. Phys. J. E.* 9:365–374.

51. Niggemann, G., M. Kummrow, and W. Helfrich. 1995. The bending rigidity of phosphatidylcholine bilayers: dependences on experimental method, sample cell sealing and temperature. *J. Phys. II France.* 5:413–425.

52. Rawicz, W., K. C. Olbrich, T. McIntosh, D. Needham, and E. Evans. 2000. Effect of chain length and unsaturation on elasticity of lipid bilayers. *Biophys. J.* 79:328–339.

53. Ratanabanangkoon, P., M. Gropper, R. Merkel, E. Sackmann, and A. P. Gas. 2002. Two-dimensional streptavidin crystals on giant lipid bilayer vesicles. *Langmuir.* 18:4270–4276.

54. Ratanabanangkoon, P., M. Gropper, R. Merkel, E. Sackmann, and A. P. Gas. 2003. Mechanics of streptavidin-coated giant lipid bilayer vesicles: a micropipette study. *Langmuir.* 19:1054–1062.

55. Gompper, G., and D. M. Kroll. 1997. Network models of fluid, hexatic and polymerized membranes. *J. Phys. Condens. Matter.* 9:8795–8834.

56. Helfrich, W. 1986. Size distributions of vesicles: the role of the effective rigidity of membranes. *J. Phys. [E].* 47:321–329.

57. Milner, S. T., and S. A. Safran. 1987. Dynamical fluctuations of droplet microemulsions and vesicles. *Phys. Rev. A.* 36:4371–4379.

58. Miao, L., U. Seifert, M. Wortis, and H.-G. Döbereiner. 1994. Budding transitions in fluid bilayer vesicles: the effect of area-difference elasticity. *Phys. Rev. E.* 49:5389–5407.

59. Rivetti, C., M. Guthold, and C. Bustamante. 1996. Scanning force microscopy of DNA deposited onto mica: equilibration versus kinetic trapping studied by statistical polymer chain analysis. *J. Mol. Biol.* 264:919–932.

60. Desingess, M.-N., B. Maier, Y. Zhang, M. Peliti, D. Bensimon, and V. Croquette. 2002. Stretching single stranded DNA, a model polyelectrolyte. *Phys. Rev. Lett.* 89:248102.

61. Smith, D. E., T. T. Perkins, and S. Chu. 1996. Dynamical scaling of DNA diffusion coefficients. *Macromolecules.* 29:1372–1373.

62. Breidenich, M., R. R. Netz, and R. Lipowsky. 2001. Adsorption of polymers anchored to membranes. *Eur. Phys. J. E.* 5:403–414.

63. Pécréaux, J., H.-G. Döbereiner, J. Prost, J.-F. Joanny, and P. Bassereau. 2004. Refined contour analysis of giant unilamellar vesicles. *Eur. Phys. J. E.* 13:277–290.

64. Lipowsky, R. 1992. Budding of membranes induced by intramembrane domains. *J. Phys. II France.* 2:1825–1840.

65. Lipowsky, R., and R. Dimova. 2003. Domains in membranes and vesicles. *J. Phys. Condens. Matter.* 15:S31–S45.

66. Nicolas, A., and B. Fourcade. 2003. Polymers grafted to a fluid and flexible membrane: extreme sensitivity to the grafting density. *Eur. Phys. J. E.* 10:355–367.

67. Evans, A., M. S. Turner, and P. Sens. 2003. Interactions between proteins bound to biomembranes. *Phys. Rev. E.* 67:041907.

68. Kim, Y. W., and W. Sung. 1999. Vesicular budding induced by a long and flexible polymer. *Europhys. Lett.* 47:292–297.